CHEMIJA. 2008. Vol. 19. No. 1. P. 25–31

Dedicated to the 80th anniversary of Professor Romanas Višomirskis

Cobalt-rich Zn–Co alloys: electrochemical deposition, structure and corrosion resistance

Svetlana Lichušina,

Ala Chodosovskaja,

Aloyzas Sudavičius,

Remigijus Juškėnas,

Dalia Bučinskienė,

Algis Selskis,

Eimutis Juzeliūnas*

Institute of Chemistry,
A. Goštauto 9, LT-01108 Vilnius,
Lithuania

Cobalt-rich Zn–Co alloy coatings (e. g., Zn–15Co, Zn–18Co) were electrodeposited from an alkaline electrolyte under anomalous (at high current densities) and non-anomalous (at low current densities) co-deposition conditions. The fibre nanostructures consisting of ca 94% of Co were deposited under certain conditions. X-ray diffraction (XRD) measurements confirmed that the alloy structure consisted of single gamma-phase Co_5Zn_{21}. Electrochemical impedance spectroscopy (EIS) showed that corrosion resistance of the cobalt-rich alloys at the initial corrosion stages was about three times as high as that of pure Zn and comparable to the corrosion resistance of pure Co. Tests in salt fog (until red rust) revealed up to four times higher corrosion resistance of cobalt-rich alloys as compared to that of the conventionally used Zn–1Co alloy. The morphological properties and the chemical composition of corrosion products were studied by atomic force microscopy (AFM) and X-ray photoelectron spectroscopy (XPS). Zinc was found to be in an oxidized state within a corrosion product layer, whereas cobalt was not oxidized. Based on this, a cobalt-enriched protective layer forming during the corrosion process was assumed. The results demonstrated that Co-rich coatings, owing to their high corrosion resistance, may be considered as a replacement for chromated coatings (Zn, Co-poor alloys) or Zn–Ni.

Key words: Zn–Co alloys, electroplating, corrosion resistance

INTRODUCTION

Zn–Co alloys with low contents of Co (usually about 1% in mass) have superior corrosion resistance when compared to pure zinc [1–4]. The effect is especially pronounced when the samples are additionally protected by conversion coatings. Although the first publication on cobalt's inhibiting effect appeared more than two decades ago, the subject still attracts considerable attention of researchers [5–18]. Nevertheless, the inhibiting effect is not well understood and the concepts seem to be ambiguous.

Vilche et al. attributed the corrosion inhibition to the chemical stabilization of the oxide film and retardation of ion transportation or vacancies within the passive layer developed during the corrosion process [19]. Kautek et al. explained the corrosive activity suppression by the elimination of the negatively charged zinc cation vacancies by cobalt [20]. Ramanauskas came to a conclusion that structural properties of the alloy were of substantial importance to the superiority of corrosion resistance [21]. The role of the corrosion products developed on the alloy surface has also been investigated [22, 23]. It has been assumed that the amorphous structure of the corrosion product layer developed during atmospheric corrosion may play an important role in the corrosion resistance [23].

* Corresponding author. E-mail: ejuzel@ktl.mii.lt

The co-deposition process of Zn and Co was observed to be anomalous in many cases, as the deposition of less noble Zn is preferential to the deposition of more noble Co. Various explanations of the anomaly were suggested, e. g., underpotential co-deposition (UPD), kinetic behaviour of both components, the hydroxide suppression mechanism and the influence of Co(III).

According to UPD hypothesis, the co-deposition proceeds continuously on an alloy surface that is different from the parent metals and, therefore, the deposition of a less noble component is preferential [24]. A complex cathodic peak in the region of zinc UPD indicated the deposition of cobalt-rich alloys [8]. These experiments showed a remarkable increase in Zn content (gamma phase) in the region between the UPD cathodic peak potential and that of Zn bulk deposition.

The anomalous co-deposition was explained by certain types of kinetic behavior and difference in the exchange current densities [25–27]. The retardation effect was also attributed to zinc hydroxide included in the alloy matrix [28], though AES and XPS measurements did not provide evidence for the inclusion of zinc hydroxide in the alloy deposit [29].

As regards anomalous co-deposition of iron–nickel alloys, a certain hydroxide suppression mechanism was suggested by Dahms and Croll [30]. A rise in pH in the vicinity of the electrode occurs due to the hydrogen evolution, which causes precipitation of zinc hydroxide on the surface, which prevents the deposition of

cobalt, whereas zinc may deposit readily from the adsorbed layer [31]. The initial stages of zinc and zinc–cobalt alloy deposition were investigated by electrochemical quartz crystal microbalance (EQCM), which provided precise data on the electrode mass change *in situ* [32]. The initial mass growth was several times higher than that predicted by Faraday's law under both pulse and constant current conditions. The result implies the precipitation of barely soluble compounds during the initial stages of electrolysis. With an increase in the electrolysis time, however, the process may change to normal as was shown by Gomez and Valles [33]. No reduction of zinc and no precipitation of zinc oxide / hydroxide were concluded from SEM analysis at –1000 mV (SCE) [34]. At more negative potentials, zinc deposition occurred after an incubation period. The authors suggested a hydroxide oscillation model for Zn–Co deposition, according to which a formation and decay of the colloidal zinc hydroxide layer takes place during the deposition.

The importance of Co(III) ions forming on the anode due to the oxidation of Co(II) was discussed by Bahroloom et al [35]. The authors concluded that the trivalent ions prevent the deposition of Co-rich alloy coatings. The co-deposition mechanism changed from anomalous to equilibrium and high cobalt concentrations were deposited when the influence of the trivalent ions was prevented using a two-compartment cell.

While Zn alloys with low Co contents were substantially investigated, relatively little is known about the system with a higher cobalt concentration. Some studies have been performed on the properties of Zn–Co alloys under pulse plating conditions [12, 13, 18]. Compositions with high Co concentrations (up to 90%) were deposited by selecting current density and pulse plating waveforms. Electrodeposits with high cobalt content were obtained in the alkaline electrolyte [36]. The authors focused on the relation between heat treatment and changes in the structure and corrosion behaviour of the deposits. The heat treated specimens were more active than the non-treated alloys.

The present study aims at depositing of Co-rich Zn–Co alloys, the corrosion resistance of which could be comparable to that of conventionally used Co-poor alloys protected by chromate conversion coatings. Since the application of chromates became increasingly restricted due to environmental regulations, the alloys of superior corrosion resistance could be considered as an alternative for the application of chromate conversion coatings. Highly resistant Zn–Co alloys could be also considered as an alternative to Zn–Ni alloys as nickel sometimes may be less desirable (e. g., due to allergenic factors) than cobalt.

EXPERIMENTAL

The electrolyte was prepared using analytical class purity reagents $CoSO_4 \times 7H_2O$, ZnO, NaOH, a complexing agent [37] and triply distilled water. Zn–Co alloy coatings were deposited on steel plates (S = 1 cm^2), which were pre-treated with emery paper (grade 2500) and MgO powder, rinsed with 5% HCl and finally with distilled water.

The alloy composition analysis by XPS was performed after surface etching by ionised argon. Photoelectron spectra were recorded by an 'Escalab MK II' spectrometer using X-ray radiation of MgK_α (1253.6 eV, pass energy 20 eV). The pressure 1.33×10^{-6} Pa was kept in an UHV analysis chamber. The etching was performed in the preparation chamber at vacuum of 6×10^{-3} Pa for 60 s, accelerating voltage 6.0 kV and beam current 100.0 μA cm^{-2} (this corresponded to an etching rate of ca 10 nm min^{-1}). Co $2p_{3/2}$, Zn $2p_{3/2}$, O 1s spectra and Auger Zn $L_3M_{45}M_{45}$ spectra were recorded.

X-ray diffraction (XRD) measurements were performed using a 'Bruker D8' diffractometer equipped with a Göbel mirror (primary beam monochromator) for Cu radiation. A continuous scan mode was used in a range of $30° < 2\Theta < 75°$ with a scan rate of 1° min^{-1}. The crystallite size D was estimated from the peak width at half of the maximum peak intensity b using the well-known Scherrer equation.

Atomic force microscopy (AFM) measurements were conducted using a 'TopoMetrix Explorer SPM'. The images were obtained with a Si_3N_4 tip in a contact mode.

Impedance measurements were carried out using an IM6 apparatus from 'Zahner'. The signal amplitude was 10 mV.

The corrosion resistance of the deposited alloys was evaluated in a neutral 5% NaCl salt fog. The specimens were exposed in a salt spray chamber ('Q-Panel') in accordance with standard ISO 10289 : 1999. The thickness of the coatings used for the corrosion testing was 10 μm.

Different methods, such as X-ray photoelectron spectroscopy (XPS), X-ray diffraction (XRD), scanning electron microscopy (SEM) and atomic absorption spectroscopy (AAS), were compared by their suitability to study Zn–Co alloy composition. The percentage of cobalt c_{Co} (%) in the deposit was calculated having divided the mass of cobalt (m_{Co}) by the mass of both elements m_{Co+Zn}:

$$c_{Co}(\%) = (m_{Co} / m_{Co+Zn}) \times 100. \quad (1)$$

Close concentration values of cobalt were found using different method: AAS – 14%, SEM – 14%, XRD – 17%, and the average value was $c_{Co} \approx 15\%$ for the alloy deposited at 10 mA cm^{-2}. XPS analysis gave $c_{Co} \approx 15$–20% depending on the depth (sputtering time). It should be noted that the XPS determining is complicated because the analysis is related to the surface layer, and it always contains some oxygen (even after surface sputtering by Ar^+, a part of the surface may be re-oxidized by the oxygen released from oxides). Another complication may appear due to a non-uniform surface etching by Ar^+.

RESULTS AND DISCUSSION

Data on the Co concentration in the alloy depending on current density and Co(II) concentrations in the electrolyte are given in Fig. 1. Composition reference lines (CRL) indicate the concentration ratio Co(II) / [Co(II) + Zn(II)] in the solution. The Co concentration in the alloy, which exceeds CRL, means a normal co-deposition, while the content below the line means an anomalous co-deposition (the deposition of less noble Zn is preferential). Obviously, the co-deposition process is normal at lower current densities, while it changes to the anomalous one when increasing the current density. Possible reasons of the anomaly were referred to in the introduction section.

Microtopography of the alloy surfaces deposited under constant and pulsed current conditions is demonstrated on the

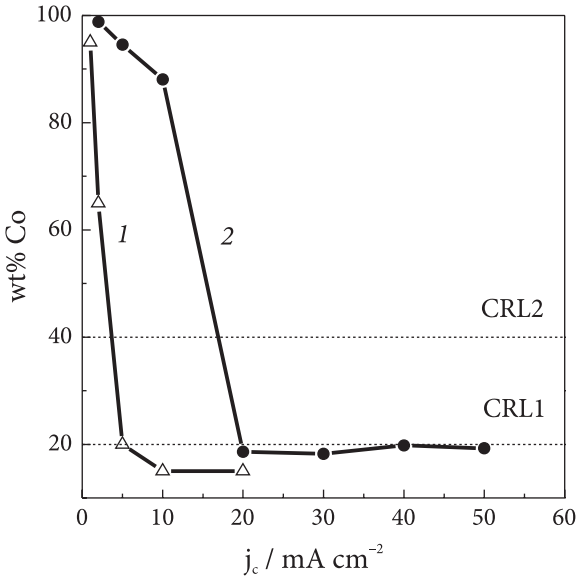

Fig. 1. Content of Co in alloy deposit in mass % depending on current density and Co(II) concentration in the electrolyte. Co(II) concentration in the electrolyte: *1* – 35 mM, *2* – 70 mM. Zn(II) concentration – 0.12 M, complexing agent concentration: 0.19 M *(1)* and 0.38 M *(2)*. The composition reference lines (CRL) indicate the codeposition type: anomalous – below the corresponding CRL line and normal – above the line

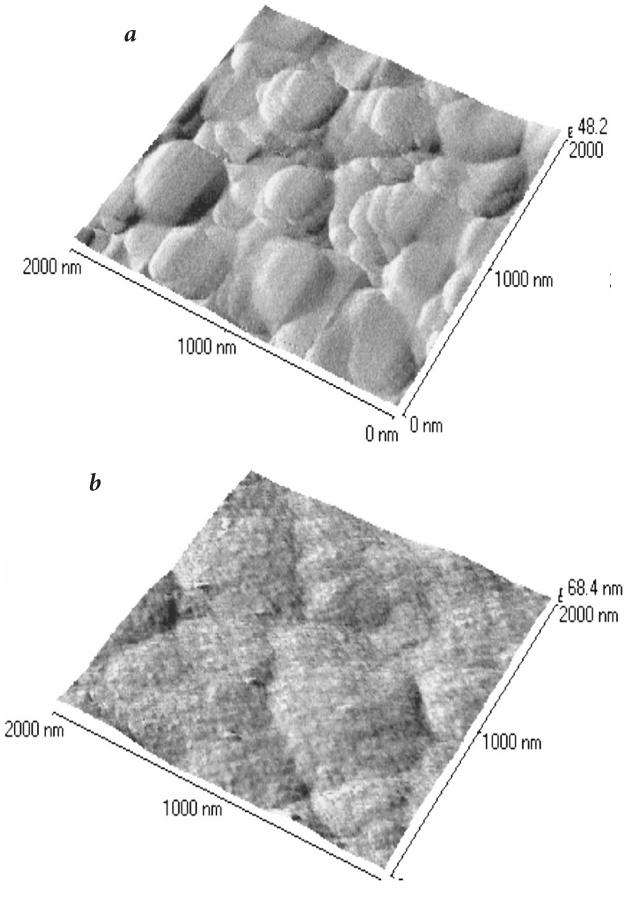

Fig. 2. Microtopography of Zn–Co coatings deposited by constant and pulse (t_{on} / t_{off} = 1/10 ms) currents from the electrolyte: Co(II) – 35 mM; Zn(II) – 0.12 M; NaOH – 2.5 M; complexing agent – 0.19 M. Constant current density 10 mA cm^{-2} (*a*); pulse current 220 mA cm^{-2} (*b*). Cobalt concentration in the coatings (in mass): *a* – 15%, *b* – 16%

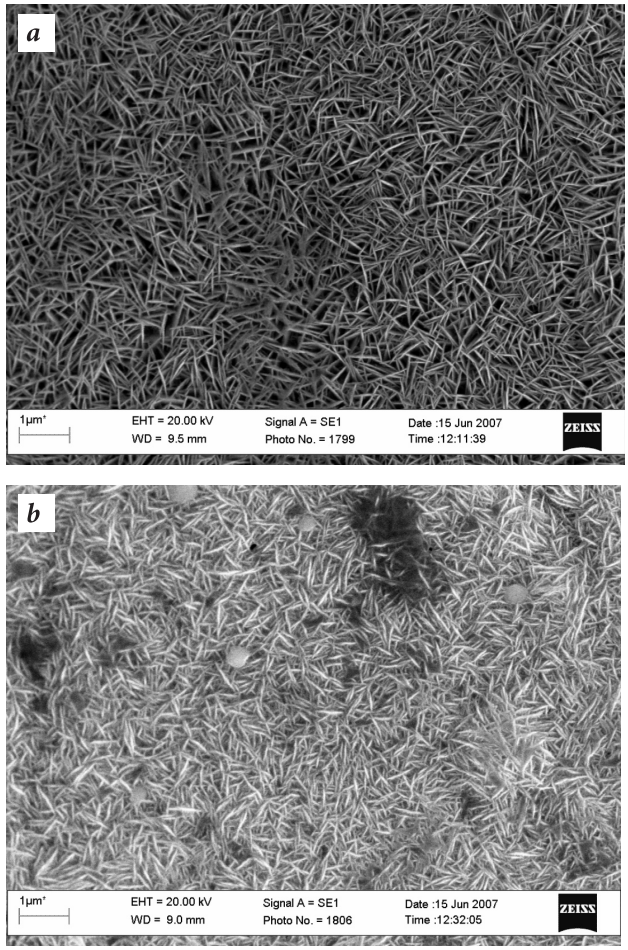

Fig. 3. SEM images showing the surface morphology of Zn–Co coatings deposited from the electrolyte: Co(II) – 70 mM; Zn(II) – 0.12 M; NaOH – 2.5 M; complexing agent – 0.38 M. Current density in mA cm^{-2}: 2 (*a*); 5 (*b*). Cobalt concentration in the coatings (in mass): 98.81% (*a*); 94.55% (*b*)

atomic force microscopy (AFM) images (Fig. 2). A surface composed of the formations, the size of which is in the order of several hundred nanometres, is typical of the deposits obtained under constant current conditions. No significant differences in the morphology for different current density values were observed (data not shown). Larger formations were formed when applying a high pulsed current, e. g., $j_{c,p}$ = 220 mA cm^{-2} with the Co content 16% (Fig. 2b). It is interesting that a fine structure (nanostructure) is present on the pulse-plated surfaces. Presumably, this structure is build from hydroxide precipitates and forms at higher current densities and has been discussed when analysing the reasons for the anomalous co-deposition [30–32].

SEM images on Fig. 3 show interesting fibre-like structures, which deposit on steel when applying low current densities. The deposits consist of very high content of cobalt (94–99%). These remarkable structures may be attractive when attempting to develop cobalt oxide-based super-capacitors. Recently, attempts are focused on the development of alternatives to the super-capacitors made of expensive materials such as ruthenium dioxide. What is most important here is to find alternative materials with very high surface area (high capacitance).

The results of the structural studies by XRD are shown in Fig. 4. At low current densities and high cobalt content (e. g.,

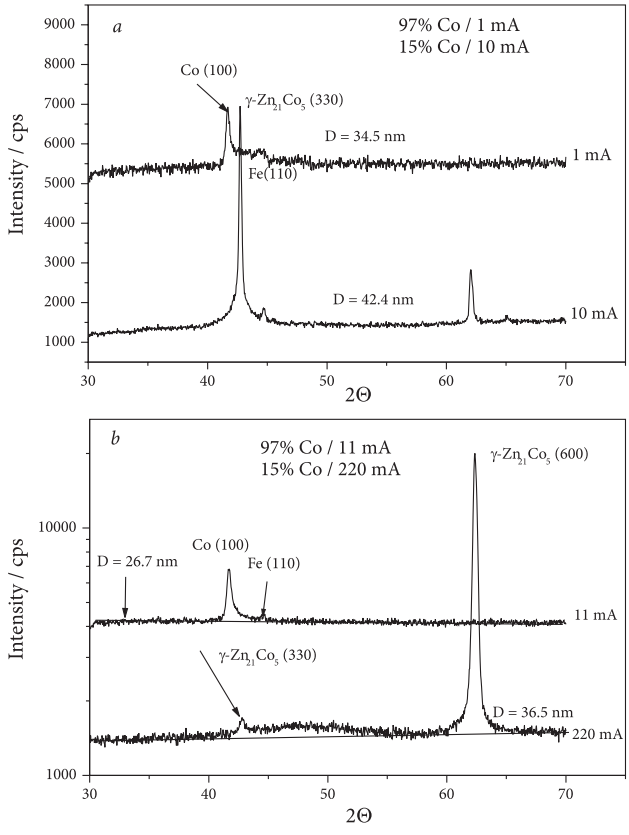

Fig. 4. XRD study of Zn–15Co alloy deposited under constant (*a*) and pulsed current (*b*) conditions from the electrolyte: Co(II) – 35 mM; Zn(II) – 0.12 M; NaOH – 2.5 M; complexing agent – 0.19 M. The current densities are indicated on the figure, $t_{on} / t_{off} = 1/10$ ms

$j_c = 1$ mA cm^{-2} and $c_{Co} = 97\%$), the diffraction pattern indicates a hexagonal Co structure. At higher current densities (lower Co concentration), a cubic body-centred gamma-phase Co_5Zn_{21} is deposited under both constant and pulsed currents (Fig. 4 a, b). The grains are weakly textured in direction <110>. The grain size increases with the current density: $D = 34.5$ nm at $j_c = 1$ mA cm^{-2} and $D = 42.4$ nm at $j_c = 10$ mA cm^{-2} (Fig. 4 a) and $D = 26.7$ nm at $j_c = 11$ mA cm^{-2} and $D = 36.5$ nm at $j_c = 220$ mA cm^{-2} (Fig. 4 b). An outspread maximum around a wide region of diffraction angle $2\Theta = 40°–55°$ is observed for the deposits obtained under the pulsed current conditions (220 mA cm^{-2}, Fig. 4 b). This indicates an amorphous structure to be formed by the pulsed current. Quite probably, the same fine structure is observed on AFM images as well (Fig. 2).

The gamma-phase Co_5Zn_{21} alloy structure deposited by the constant current gives grounds to predict high corrosion stability of the alloy. As it is commonly known, the gamma-phase structure is characteristic of high corrosion resistance, and the absence of additional phases is favourable to alloy stability.

XPS and surface etching by ionized argon were applied to analyze the metals within the corrosion product layer (Fig. 5). The samples were pre-exposed for 48 hours in a naturally aerated 3.5% NaCl solution. The spectra of Co $2p_{3/2}$ allow distinguishing between the non-oxidized metal (binding energy is $E_b = 777.9$ eV) and the oxidized one ($E_b = 780.0$ eV). Such discrimination is problematic for zinc as the Zn $2p_{3/2}$ spectra are similar for both the non-oxidized and the oxidized metals

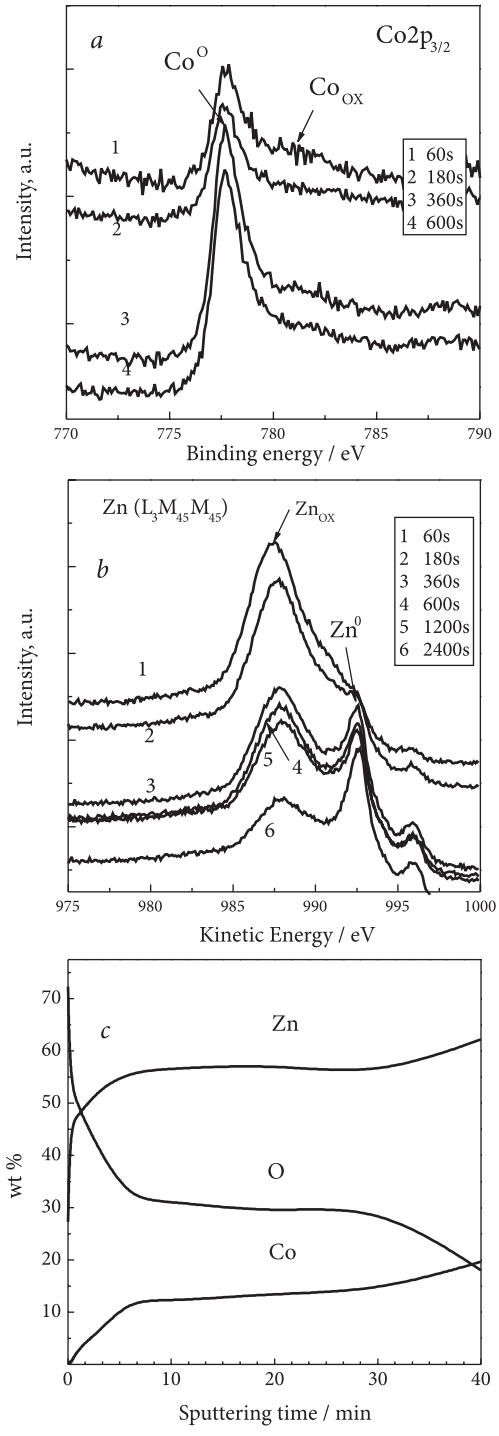

Fig. 5. X-ray photoelectron spectra (XPS) for Co $2p_{3/2}$ region of Zn–20Co alloy sample after various sputtering times (*a*), Auger Zn $L_3M_{45}M_{45}$ spectra (AES) of the same Zn–20Co alloy sample after various sputtering times (*b*) and depth profiles (XPS) of Zn, Co and O (*c*) for Zn–20Co alloy exposed for 48 hours in 3.5% NaCl solution

(1021.6 eV and 1021.7 eV, respectively). To solve this problem, Auger spectrum of Zn(L3M45M45) was recorded (the kinetic energy for Zn is 992.3 eV, while the energy for ZnO is 987.6 eV).

According to the electron energy peaks, cobalt was found within the outer layer in the non oxidized form (Co^0), while zinc was in the oxidized one (Zn_{ox}). Only traces of Co_{ox} and Zn^0 are present at a depth of 10 nm (Fig. 5, sixty-second etching,

curve 1). In deeper levels, some Zn_{ox} appears as indicated by the energy peak at 992 eV. Cobalt, however, was found to be non-oxidized within the concentration profile studied. This result implies that the corrosion of zinc, as a less noble component, is prevailing during the first corrosion stages, whereas more noble cobalt remains non-corroded (i. e. a de-alloying process takes place). Consequently, a part of the surface layer must be enriched with cobalt (the more corrosion resistant component), and this, in turn, may lead to a superior corrosion resistance when compared with that of the non-corroded counterpart. The increased content of cobalt within the corrosion product layer was also confirmed by calculations. The Zn / Zn^{++} ratio was found from the areas of the corresponding spectra (Fig. 5 b), and further the percentage of Co with respect to the total mass of Co + Zn was derived. It was calculated that the surface after 6 min of sputtering contained twice as high Co concentration as that of the bulk alloy (i. e. 31% vs 15%, respectively).

It should be noted that XPS method has serious limitations for the detection of perfectly layered structures (interfaces) on corroding metals and alloys. The main complication arises from the non-uniformity of etching of highly non-homogeneous surfaces. Furthermore, the measurements are performed *ex-situ* under vacuum conditions, which are quite different from those in a corrosive environment.

The corrosion rate, by definition, is determined by the electron transfer kinetics through a system of charged interfaces and different types of conductors: electronic (metal), semiconductor (corrosion product layers) and ionic (solution containing dissolved oxidisers and corrosion products). The corrosion current density (j_{corr}, A cm^{-2}), according to a well-known ratio, is in inverse proportion to the polarization resistance (R_p, Ω cm^2) [38]. The latter can be determined from the voltammetric dependence as the ratio between the potential (E) and the current density (j) close to the open circuit potential [$R_p = (\Delta E / \Delta j)_{\Delta E \to 0}$], i. e. in the region, where the voltammetric dependence could be approximated as a rectilinear one. Impedance (Z) measurements at low frequency (ω) domain ($R_p = Z_{\omega \to 0}$) or the equivalent circuit parameters used for the experimental data fitting provide another possibilities to obtain R_p. The results of EIS studies are given in Fig. 6.

The EIS data given in Fig. 6 show the data change over the exposure time in 3.5% NaCl: 10 min (1), 48 h (2) and 290 h (3).

Curve (1) relates to the initial corrosion stages with a relatively thin corrosion product layer. Pure Zn and Co were studied under analogous conditions as well. The EIS spectra fit well to a rather simple equivalent circuit, which consists of an R_t–*CPE* element (charge transfer resistance – constant phase element) and solution resistance (R_Ω) in series (insertion in Fig. 6). It should be noted that the constant phase element consists of capacitance (C, μF cm^{-2}) and frequency dispersion (n), a dimensionless parameter ($n \leq 1$), which usually is correlated with the porosity of corrosion products. If n is close to 1, this means that CPE is most capacitive.

The derived R_p values indicated that the Zn–Co alloy exhibits much higher corrosion resistance than pure zinc ($R_{p,Zn}$ = 0.85 kΩ cm^2 vs $R_{p,Zn-15Co}$ = 2.6 kΩ cm^2) and the alloy resistance is comparable with that of pure Co ($R_{p,Co}$ = 3.8 kΩ cm^2).

At longer exposures (e. g., 48 h and 290 h), a second time constant appears on the phase shift diagrams (Fig. 6). Such behaviour of the two time constants indicates the appearance of

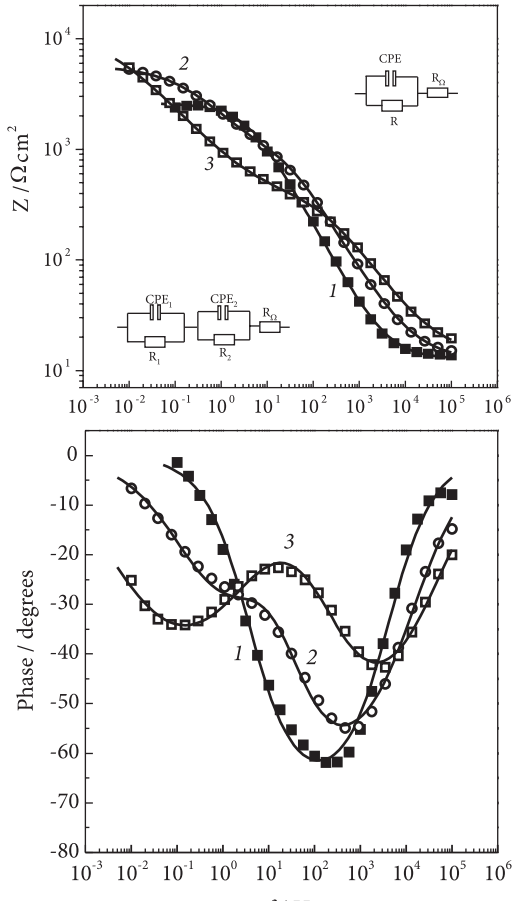

Fig. 6. EIS diagrams of Zn–15Co exposed in 3.5% NaCl solution for 10 min (*1*), 48 h (*2*) and 290 h (*3*). The experimental results (symbols) were fitted (lines) assuming the shown equivalent circuits, and the fitting parameters are as follows: (*1*) R = 2.6 KΩ cm^{-2}, C = 4.3 μF (n = 0.76); (*2*) R_1 = 5.0 KΩ cm^{-2}, C_1 = 4.7 μF (n = 0.58), R_2 = 0.7 KΩ cm^{-2}, C_2 = 3.6 μF (n = 0.77); (*3*) R_1 = 0.33 KΩ cm^{-2}, C_1 = 1.4 μF (n = 0.64), R_2 = 12 KΩ cm^{-2}, C_2 = 8 μF (n = 0.52)

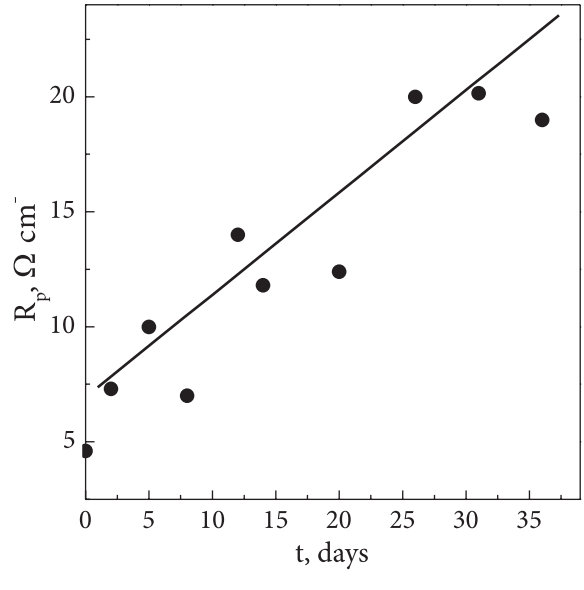

Fig. 7. Dependence of corrosion resistance (R_p) on the immersion time in 3.5% NaCl solution. Zn–18Co coating deposited at i_c = 20 mA cm^{-2}

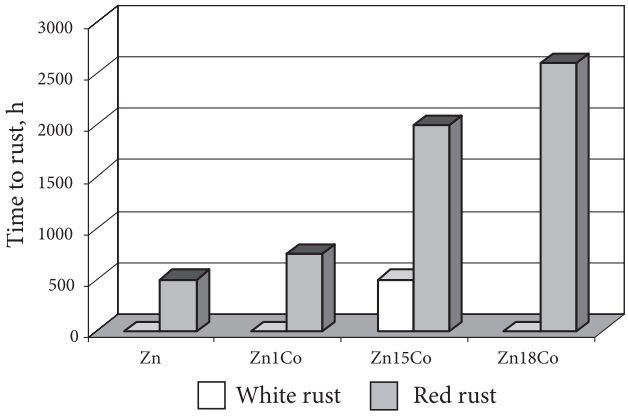

Fig. 8. Time for the appearance of white and red rust in salt fog for Zn and Zn–Co alloys. White rust appearance time, h, for: Zn – 2; Zn–1Co – 2; Zn–15Co – 500, Zn–18Co – 2

a two-layered structure on the corroding specimen. The detection by EIS and the analysis of layered structures of corrosion products was discussed elsewhere [39–43]. The corresponding equivalent circuit is shown as insertion in Fig. 6 a. The charge transfer resistance and capacitances (derived from constant phase elements) were calculated as well (the data are given in the figure caption). The total charge transfer resistance reflecting the corrosion resistance is the sum of the resistances of both layers. Figure 7 shows a significant increase in the corrosion resistance during a long-term exposure in NaCl solution.

The high corrosion resistance was also proven by a standard testing procedure in a salt fog chamber (Fig. 8). The time of the appearance of red rust indicates that the corrosion resistance of Zn–18Co is about four-fold higher than that of Zn–1Co and, thus, it is comparable with the resistance of chromated Co-poor coatings. Especially great effect is observed for white rust on Zn–15Co, e. g., 2 h for Zn, 2 h for Zn–1Co and ca 500 h for Zn–15Co.

CONCLUSIONS

Zn–Co alloys with ca 15–18% Co deposited in an alkaline electrolyte under anomalous conditions exhibited good appearance and high corrosion resistance. The resistance was comparable to that of chromated conventional Zn–Co coatings with low cobalt concentrations.

The high corrosion resistance of the alloys owed to the structural properties, i. e. single gamma-phase Co_5Zn_{21}, which was confirmed by XRD measurements.

Zinc was found by XPS analysis to be present in the oxidized state within the surface layer developed during the alloy corrosion in a NaCl solution. Cobalt, however, was found to be non-oxidized. This means that a cobalt-enriched layer develops during the corrosion process, which may lead to a superior corrosion resistance.

EIS data indicated a two-layered structure of the corrosion products, which developed during long-term exposures on Zn–Co alloys in NaCl solutions. A substantial increase in the corrosion resistance during the exposure was determined from EIS measurements.

Received 25 January 2008
Accepted 29 January 2008

References

1. T. Adaniya, M. Omura, K. Matsudo, H. Naemura, *Plat. Surf. Finish*., **68**, 96 (1981).
2. E. Knaak, H. Kohler, J. Hadley, *Metalloberflache*, **39**, 139 (1985).
3. W. Siegert, J. Hadley, *Metalloberflache*, **43**, 78 (1989).
4. E. Grunwald, A. Ziman, C. Varhelyi, C. Juhos, *Galvanotechnik*, **85**, 3274 (1994).
5. J. L. Ortiz-Aparicio, Y. Meas, G. Trejo, R. Ortega, T. W. Chapman, E. Chainet, P. Ozil, *Electrochim. Acta*, **52**, 4742 (2007).
6. S. Sigamani, M. Pushpavanam, *Trans. Inst. Met. Fin*., **84**, 326 (2006).
7. E. M. K. Hiller, M. J. Robinson, *Corros. Sci*., **48,** 1019 (2006).
8. G. Roventi, T. Bellezze, R. Fratesi, *Electrochim. Acta*, **51**, 2691 (2006).
9. N. Boshkov, K. Petrov, D. Kovacheva, S. Vitkova, S. Nemska, *Electrochim. Acta*, **51**, 77 (2005).
10. J. Y. Fei, G. Z. Liang, W. L. Xin, J. H. Liu, *Chinese Chemical Letters*, **16**, 1097 (2005).
11. D. Koleva, N. Boshkov, G. Raichevski, L. Veleva, *Trans. Inst. Met. Fin*., **83**, 188 (2005).
12. J. Fei, G. Z. Liang, W. L. Xin, *Chinse J. Chem. Eng*., **13**, 259 (2005).
13. J. Y. Fei, G. D. Wilcox, *Electrochim. Acta*, **50**, 2693 (2005).
14. C. N. Panagopoulos, K. G. Georgarakis, S. Petroutzakou, *J. Mat. Process. Technol*., **160**, 234 (2005).
15. M. Pushpavanam, M. Siluvai Micael, *Trans. Inst. Met. Fin*., **82**, 174 (2004).
16. R. Ramanauskas, R. Juškėnas, A. Kaliničenko, L. F. Garfias-Mesias, *J. Solid State Electrochem*., **8**, 416 (2004).
17. E. M. K. Hiller, M. J. Robinson, *Corros. Sci*., **46**, 715 (2004).
18. M. E. Bahroloom, M. E. Gabe, G. D. Wilcox, *Trans. Inst. Met. Fin*., **82**, 51 (2004).
19. J. R. Vilche, K. Juttner, W. J. Lorenz, W. Kautek, W. Paatsch, M. H. Dean, U. Stimming, *J. Electrochem. Soc*., **136**, 3773 (1989).
20. W. Kautek, M. Sahre, W. Paatsch, *Electrochim. Acta*, **39**, 1151 (1994).
21. R. Ramanauskas, *Appl. Surf. Sci*., **153**, 53 (1999).
22. Z. M. Tu, Z. L. Yang, M. Z. An, W. L. Li, J. S. Zhang, *Trans. Inst. Met. Finish.*, **77**, 246 (1999).
23. R. Ramanauskas, P. Quintana, P. Bartolo-Perez, L. Diaz-Ballote, *Corrosion*, **56**, 588 (2000).
24. M. J. Nicol, H. I. Philip, *J. Electroanal. Chem*., **70**, 233 (1976).
25. M. F. Mathias, T. W. Chapman, *J. Elecrochem. Soc*., **134**, 1408 (1987).
26. D. Landolt, *Electrochim. Acta*, **39**, 1075 (1994).
27. Z. L. Li, J. L. Cai, S. M. Zhou, *Trans. Inst. Met. Finish.*, **77**, 149 (1999).
28. Y. M. Loshkarev, V. I. Korobov, V. V. Trofimenko, F. A. Chmilenko, *Prot. Met*., **30**, 79 (1994).
29. D. E. O. S. Carpenter, M. Ashworth, J. P. G. Farr, *Trans. Inst. Met. Finish.*, **81**, 177 (2003).
30. H. Dahms, I. M. Croll, *J. Elecrochem. Soc*., **112**, 771 (1965).

31. K. Higashi, H. Fukushima, T. Urakawa, T. Adaniya, K. Matsudo, *J. Electrochem. Soc*., **128**, 2081 (1981).
32. A. Stankevičiūte, K. Leinartas, G. Bikulčius, D. Virbalytė, A. Sudavičius, E. Juzeliunas, *J. Appl. Electrochem*., **28**, 89 (1998).
33. E. Gomez, E. Valles, *J. Electroanal. Chem*., **397**, 177 (1995).
34. H. Yan, J. Downes, P. J. Boden, S. J. Harris, *J. Electrochem. Soc*., **143**, 1577 (1996).
35. M. E. Bahroloom, M. E. Gabe, G. D. Wilcox, *J. Elec-trochem. Soc*., **150**, C144 (2003).
36. A. Cunha, S. D. Carpenter, J. Z. Ferreira, D. E. O. S. Carpenter, J. P. G. Farr, *Corros. Eng. Sci. Technol*., **38**, 313 (2003).
37. S. Lichusina, E. Juzeliūnas, Patent No 5481, Lithuania (2006).
38. M. Stern, *J. Electrochem. Soc*., **102**, 609 (1955).
39. J. R. Vilche, F. E. Varela, G. Aguna, E. N. Codaro, B. M. Rosales, A. Fernandez, G. Moriena, *Corros. Sci*., **37**, 941 (1995).
40. E. Juzeliūnas, R. Ramanauskas, A. Lugauskas, K. Leinartas, M. Samulevičienė. A. Sudavičius, R. Juškėnas, *Corrosion Sci*., **49**, 4098 (2007).
41. E. Juzeliūnas, R. Ramanauskas, A. Lugauskas, M. Samulevičienė, A. Sudavičius, *Electrochim Acta*, **51**, 305 (2005).
42. E. Juzeliūnas, R. Ramanauskas, A. Lugauskas, M. Samulevičienė, K. Leinartas, *Electrochem. Commun*., **7**, 305 (2005).
43. P. Kalinauskas, I. Valsiūnas, M. Samulevičienė, E. Juzeliūnas, *Corros. Sci*., **43**, 2083 (2001).

Svetlana Lichušina, Ala Chodosovskaja, Aloyzas Sudavičius, Remigijus Juškėnas, Dalia Bučinskienė, Algis Selskis, Eimutis Juzeliūnas

Zn–Co LYDINIAI SU DIDELIU KOBALTO KIEKIU: ELEKTROCHEMINIS NUSODINIMAS, STRUKTŪRA IR KOROZINIS ATSPARUMAS

S a n t r a u k a

Zn–Co lydinio dangos su daug kobalto (Zn–15Co, Zn–18Co) buvo nusodinamos iš šarminio elektrolito esant anomaliam sąsėdžiui (kai srovės tankiai dideli) ir kai sąsėdis nėra anomalus (esant mažiems srovės tankiams). Esant mažiems srovės tankiams nusodinamos dangos, kurių sudėtyje yra 94 sv.% Co, pasižyminčios nanostruktūra. Rentgeno spindulių difrakcijos metodu nustatyta, kad lydinį sudaro tik γ-Co_5Zn_{21} fazė. Elektrocheminio impedanso spektroskopijos metodas parodė, kad korozijos pradžioje lydinių su daug Co atsparumas korozijai beveik tris kartus didesnis, palyginus su gryno Zn atsparumu korozijai, ir prilygsta gryno Co atsparumui korozijai. Bandymai korozijos kameroje parodė, kad lydinys su daugiau kobalto keturis kartus atsparesnis korozijai, lyginant su įprastiniu Zn–1Co lydiniu. Korozijos produktų morfologija ir cheminė sudėtis buvo tirta atominės jėgos mikroskopijos ir rentgeno fotoelektroninės spektroskopijos metodais. Nustatyta, kad Zn korozijos produktų sluoksnyje yra oksiduotos būsenos, tuo tarpu Co yra metalinis. Tyrimai parodė, kad korozijos proceso metu susidaro kobaltu praturtintas apsauginis sluoksnis. Gauti duomenys leidžia daryti išvadą, kad kobaltu praturtintos dangos dėl jų didelio atsparumo korozijai gali pakeisti chromatuotas dangas (Zn, Zn su nedaug Co) arba Zn–Ni.